Composites: Part A 87 (2016) 131–137

Contents lists available at ScienceDirect

Composites: Part A

journal homepage: www.elsevier.com/locate/compositesa

Quantification of micro-scale variability in fibre bundles

F. Gommer [a,b,*], A. Endruweit [a], A.C. Long [a]

[a] Composites Research Group, Faculty of Engineering, University of Nottingham, University Park, Nottingham NG7 2RD, UK
[b] Department of Aeronautics, Imperial College London, South Kensington, London SW7 2AZ, UK

ARTICLE INFO

Article history:
Received 12 January 2016
Received in revised form 7 April 2016
Accepted 19 April 2016
Available online 20 April 2016

Keywords:
A. Carbon fibres
B. Microstructures
C. Statistical properties/methods
D. Optical microscopy

ABSTRACT

Local variations in the random filament arrangement in carbon fibre bundles were determined by optical microscopy and automated image analysis. Successive steps of abrading, polishing and acquiring micrographs of the sample surface made it feasible to analyse the micro-structure over a series of cross-sections along the fibre bundle path. Random and systematic changes in local filament arrangements were determined. Systematic changes were related to the interaction of a fibre bundle with an intersecting binder thread leading to a local increase of the fibre volume fraction at the interface. Random clustering of filaments in areas of high or low fibre volume fractions within the fibre bundles were found to be unaffected by the relative position of the bundle.

1. Introduction

Textile reinforcements utilised in the manufacture of composite components are based on filaments which are usually bundled in yarns and then processed into a fabric for easier handling. Due to this structure, fibre reinforced components are usually analysed on different levels, each with its own variability. Composite parts are made from layers of textile reinforcement (macro-scale) which consist of individual fibre bundles (meso-scale). The bundles can consist of several thousand filaments (micro-scale). It was shown that the variability at each scale affects the properties of a fibre reinforced composite component [1,2]. Depending on the scale of analysis, properties at the smaller scales of the material are usually homogenised, and any variability at these scales is ignored [3]. Attempts have been made to incorporate statistical variability at the smaller scales in multi-scale modelling approaches [4]. The variabilities are, however, usually obtained from randomly generated distributions only and are uncorrelated to the actual variability in the material.

For numerical analysis, fibre reinforcements are often represented by an idealised geometry of the smallest repeat in form of a unit cell [5]. To add variability of fibre bundle paths at the meso-scale, representative volume elements can be utilised [6]. In this case, the bundle paths exhibit a defined degree of variability; however, the geometry at the boundaries is usually periodic. As composite components are made from several layers of fibre reinforcement, this can introduce additional sources of variability. The stacking process introduces variability in between layers such as nesting or fibre bundle shape changes. Attempts were made to incorporate these bundle deformations into a geometrical model [7]. For the analysis of properties at the meso-scale, the filament arrangements at the micro-scale within the fibre bundles are usually treated as uniform [8]. The properties at the micro-scale are then easily estimated from bulk parameters such as the overall fibre volume fraction, V_f [9] in the yarn. Treating the fibre bundles as homogenous material ignores, however, any information about the local arrangement [10] or waviness [11,12] of the filaments. It was demonstrated numerically that the macro- or meso-scale failure of a part may be initiated by local stress concentrations at the micro-scale [13]. The local arrangements of filaments in fibre bundles should therefore not be ignored, but a systematic description is currently not available.

This paper analyses low crimp carbon fibre bundles and local effects of the reinforcement geometry on the micro-scale filament arrangements. Non-destructive examination methods such as micro-computed tomography are only feasible on very small samples and have a limited resolution [14,15]. Conventional optical microscopy is therefore used as an inexpensive alternative technique which also allows achieving a higher resolution. Automatic image analysis of optical micrographs of cross-sections of the material allows a detailed analysis in a time efficient manner [16]. The obtained data can be employed in multi-scale modelling approaches, for example, to improve the accuracy of local properties assigned to voxels in a finite element analysis [17].

* Corresponding author at: Composites Research Group, Faculty of Engineering, University of Nottingham, University Park, Nottingham NG7 2RD, UK.
E-mail address: F.Gommer@imperial.ac.uk (F. Gommer).

http://dx.doi.org/10.1016/j.compositesa.2016.04.019
1359-835X/

2. Materials and methods

2.1. Fibre reinforcement and processing

Composite panels with dimensions 125 mm × 60 mm were made from a single layer of low-crimp plain weave reinforcement and a low viscosity epoxy resin system. The fabric consisted of aligned carbon fibre bundles with a filament count of 12 K (warp direction), stabilized by thin glass fibre weft yarns coated with a thermoplastic polymer (Fig. 1). The dry fabric was placed in a stiff metallic tool where the global fibre volume fraction, V_f, is determined by the cavity height and was estimated to be 0.45. The fabric was saturated with a liquid resin matrix, MVR 444 supplied by the Advanced Composites Group, by circumferential injection at 2 bar pressure. The resin was preheated to 70° before the injection pressure was applied which reduced the initial viscosity to approximately 0.025 Pa s.

2.2. Sample preparation and image processing

Micrographic analysis of cross-sections of these specimens, cut perpendicular to the nominal fibre bundle path, allowed to identify the filament distribution within the carbon fibre bundles (Fig. 2). By successively removing thin layers of material at the surface of these specimens and acquiring new images, the filament arrangement can be determined at different positions along the fibre bundle path [18].

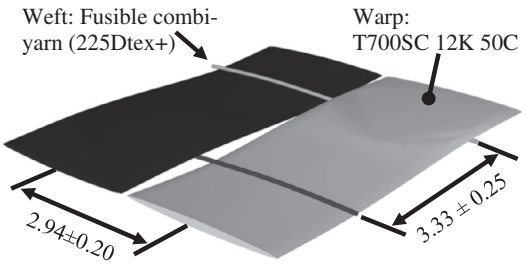

Fig. 1. Unit cell model of low-crimp plain weave, generated with the open source software TexGen available from http://texgen.sourceforge.net/. The measurements given are in mm and correspond to Ends/10 cm = 34 ± 2.5 and Picks/10 cm = 30 ± 2.5.

Stitching of overlapping images (Fig. 2C) allows large area images of fibre bundle cross-sections to be studied at high resolution [19,20]. A stitching code was implemented based on fast-Fourier correlations programmed in Matlab [21]. Micrographs were acquired at a high magnification which resulted in a pixel size of 0.09 μm (Fig. 2B). All individual filament cross-sections were determined by means of edge detection based on colour gradients in the images and fitting ellipses to the identified boundaries [16]. It was estimated that the fitted ellipse overestimates a filament cross-sectional area by about 3% on average.

Due to differences in material hardness between fibres and polymer matrix, the mechanical polishing process during sample preparation can cause filaments, located at the edge of the fibre bundle, to be abraded more than filaments in the bulk of the material. These filaments are therefore not within the limited depth of field of a conventional optical microscope imaging the bulk of the material. This results in blurred images of these filaments located at the bundle edge which can therefore not be detected with the employed image analysis method (Fig. 3). An additional false detection rate during image processing, e.g. over-/underestimation or non-detection of filament cross-sections within the bulk of the material, of approximately 2% was estimated. For these reasons, approximately only 11,500 filaments were detected during the image processing of a 12 K fibre bundle. For further interpretation of the results, the acquired micrographs and measured data of the detected filaments have been made publicly available [22].

3. Definition of fibre bundle descriptors

3.1. Fibre bundle boundary

The fibre volume fraction in a fibre bundle is defined by the combined cross-sectional area of all filaments divided by the entire area of the bundle. The cross-sectional areas of all filaments within a fibre bundle are determined during image analysis. The total bundle area is defined by a virtual boundary enclosing all filaments in the fibre bundle cross-section (Fig. 2C). To determine the envelop enclosing all filament cross-sections, the location of the top and bottom filament edge is determined over the width of the bundle. To avoid sudden changes in the estimated boundary, the filament locations are determined for a discrete step size. The

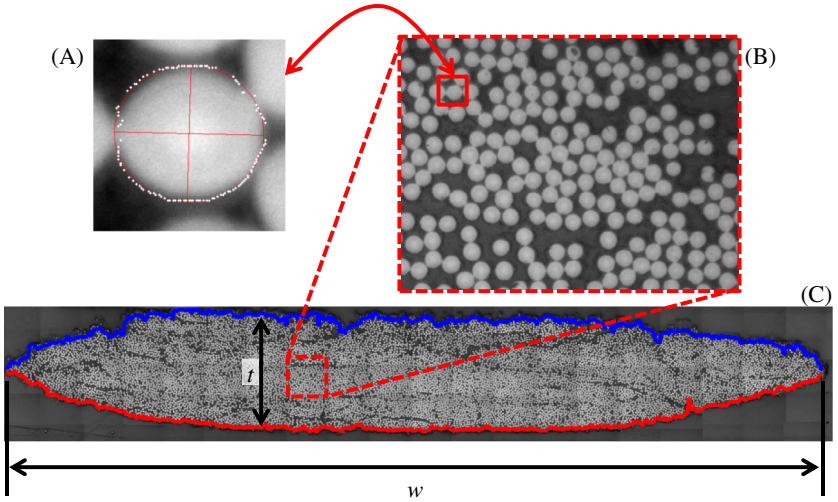

Fig. 2. (A) Filament cross-section with identified perimeter determined by image processing [16]. (B) Micrograph of carbon fibre bundle cross-section. (C) Tiling a large number of overlapping micrographs enables to analyse an entire fibre bundle. The determined fibre bundle outline is shown with solid lines and the width, w, and thickness, t, are indicated. (For interpretation of the references to colour in this figure legend, the reader is referred to the web version of this article.)

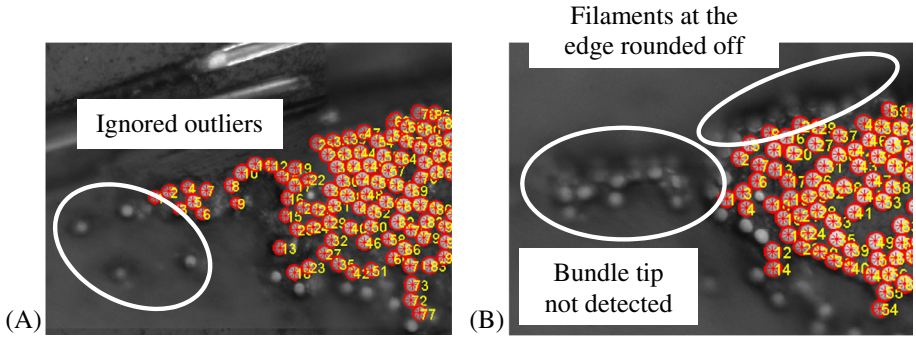

Fig. 3. Tip of a fibre bundle at two different positions in a specimen; the detected fibre bundle boundaries are marked with red ellipses. (A) Filaments separated from the bundle are ignored. (B) Problem of bundle determination due to poor image contrast at the fibre bundle tips and edges due to rounding effects. (For interpretation of the references to colour in this figure legend, the reader is referred to the web version of this article.)

width of this step size was selected to be approximately equivalent to the average diameter of the filaments. This process allows a more precise estimation of the actual fibre bundle area compared to, for example, fitting an ellipse enclosing all filaments [23].

The identified filament positions can be used to estimate the bundle width and thickness. The bundle dimensions are defined as the maximum distance along a reference direction between two filament centres on opposite sides of the fibre bundle plus one nominal filament diameter. Unlike the height, the exact determination of the bundle width usually depends strongly on the accurate detection of filaments at the narrow tips of the fibre bundles (Fig. 3). However, this accuracy may be limited due to the aforementioned problems related to the mechanical polishing process.

3.2. Fibre bundle volume fraction

The filament arrangement within fibre bundles is not uniform. A qualitative measure of the variations in local filament densities can be achieved by measuring greyscale levels in vertical and horizontal slices [24]. However, for exact quantification of the local V_f, the exact description of all filament positions is necessary [16].

After determining all filament cross-sectional areas and the bundle envelope (Fig. 4A), the fibre bundle is segmented into a finite number of vertical slices. The width of these segments was selected to be equal to 1 pixel. The absolute number of filaments detected in each slice decreases at the tips of the fibre bundle as expected (Fig. 4B). If, however, the relative amount of filaments within the fibre bundle envelop is calculated, the V_f is more uniform (Fig. 4C). A decrease in V_f towards the tips of the fibre bundle [25] could not be found. The peaks in V_f at the bundle tips occur since only a single or a very small amount of vertically arranged filaments are present, and the step size to determine the bundle boundary (Section 3.1) is smaller than the respective filament diameters. Hence, a relatively large ratio of filaments can be present in an analysed segment locally. Other artefacts, such as separations within the fibre bundle which may be caused by handling of the dry textile (Fig. 4A), decrease the absolute number of filaments locally and therefore also reduce the internal V_f in this area. Even though the V_f is relatively constant, gradual changes over the width of a fibre bundle may be present.

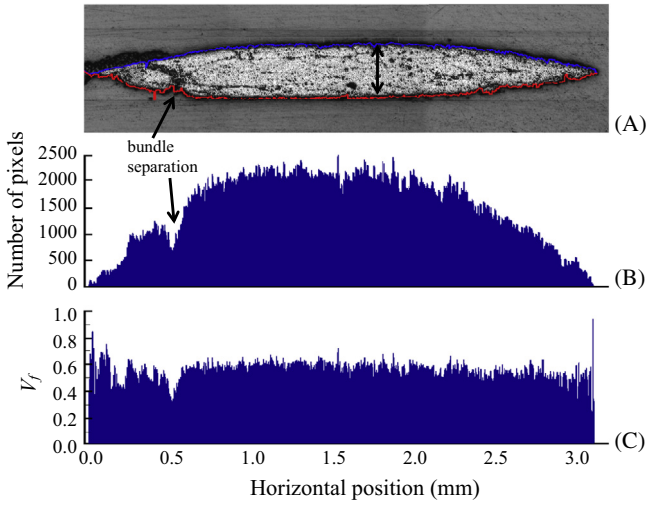

Fig. 4. (A) Fibre bundle with estimated boundaries; (B) Total filament area in pixels within the fibre bundle cross-section, estimated for vertical slices of one pixel width (δc = 0.093 μm); (C) Fibre volume fraction, V_f, within the boundaries of the fibre bundle. (For interpretation of the references to colour in this figure legend, the reader is referred to the web version of this article.)

3.3. Local fibre volume fractions

The cross-sectional area of a fibre bundle can be divided into an array of polygons by use of Voronoi cells [26]. Each point within the fibre bundle cross-section is associated to the centre point of a filament closer than any other filament centre. This results in a tessellation of the entire domain into multiple polygons (Fig. 5). The ratio of the determined filament cross-sectional area to the area of the enclosing polygon reflects the local V_f. Alternatively, the bundle could be divided into a regular grid and the V_f within each cell be calculated [27]. Unlike the Voronoi cell analysis, the V_f results would, however, depend on the selected grid size [28].

A limitation to the concept of Voronoi cell tessellation of a fibre bundle is that the analysis is based only on filament centre positions. Varying fibre diameters or apparent ellipticity of the cross-sectional areas, e.g. as a result of filament waviness inside the fibre bundle which causes filaments not to be sectioned perpendicular to their path, are ignored. The determination of the local V_f could be refined if the actual cross-sectional area of the filaments are considered [29], i.e. the Voronoi cell in this case is not dependent on filament cross-sectional centres but based on their elliptical perimeters. In this case, the Voronoi cell boundary is not any longer located equidistant between two filament centres but located half way between the closest points of two filament boundaries. In addition, the number of strongly misaligned filaments which will result in more pronounced ellipticity of individual filament cross-sections will be limited for the analysed uni-directional fibre bundles [11,12]. For analysis of the local V_f in this work, the error of ignoring the filament cross-sectional shapes for the Voronoi cell tessellation of a fibre bundle is therefore considered small as the

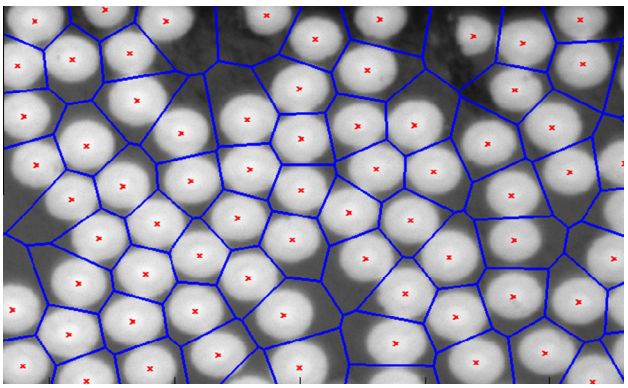

Fig. 5. Section of a micrograph of a carbon fibre bundle overlaid with polygons as a result of a Voronoi cell tessellation. (For interpretation of the references to colour in this figure legend, the reader is referred to the web version of this article.)

average misalignment of filaments is small. Hence, the variation in ellipticity of the filament cross-sections is limited and the simpler Voronoi cell tessellation based on filament centres can be used.

Attempts were made to describe the packing configuration of filaments by the Voronoi cell tessellation [30]. Voronoi polygons sharing a side with each other represent filaments which are nearest neighbours. The average number of polygon edges is therefore equivalent to the average nearest neighbour count. This method ignores, however, varying distances between filaments. The average nearest neighbour count for any fibre bundle was estimated to be 5.7. This suggests that the filaments have a tendency to be arranged in a hexagonal array (number of edges = 6) which corresponds to values reported in the literature [31,32]. However, the filaments are not necessarily arranged hexagonally (Fig. 5). Analysing the angular distribution of filament centre points between nearest neighbours, it was demonstrated that the filaments at this low V_f have the tendency to be arranged randomly [16].

4. Changes in fibre bundle composition

4.1. Fibre volume fraction variability

For two fibre bundles, a series of 12 slices (four of which are shown in Fig. 6) was imaged at successive positions over a length of about 5.3 mm. This corresponds approximately to the length of one unit cell (Fig. 1). During each re-polishing step, between 0.3 mm and 0.6 mm of material was removed. This step size is too large to reconstruct individual filament paths [11], however, it has been demonstrated that the majority of filaments in unidirectional fibre bundles only change positions within a limited cross-sectional area [12]. Hence, the effects on V_f distributions due to filament path variability between different bundle cross-sections will be limited as well.

The filament cross-sections and fibre bundle boundaries were determined for each section, and the resulting V_f (Section 3.2) are shown in Fig. 7A. It can be shown that the average V_f is not constant and varies significantly over the analysed bundle segments. In areas where a transverse binder yarn is present, V_f increases. As single layers of material were analysed at a constant mould cavity height, the compaction force acting on the fibre bundles in this area increases. This results in a compaction of the filaments locally, and hence in a local increase in V_f. The value of V_f and the fibre bundle height have therefore opposite trends (Fig. 7A and B). In areas where the fibre bundles are only compacted by the mould tool, the V_f is lower and the bundle thickness higher. The maximum peak height of V_f depends also on the bundle width (Fig. 7C). At the same height, a more narrow fibre bundle will have a higher V_f. The changes in fibre bundle width are, however, gradual and hardly affected by local bundle compaction. This suggests that changes in width of a fibre bundle are more affected by the initial state during processing. A similar effect was found when analysing the aspect ratios of bundle dimensions in a twill weave composite, which suggest the bundle width to be fairly constant over the length of two unit cells [33]. It should mentioned that the

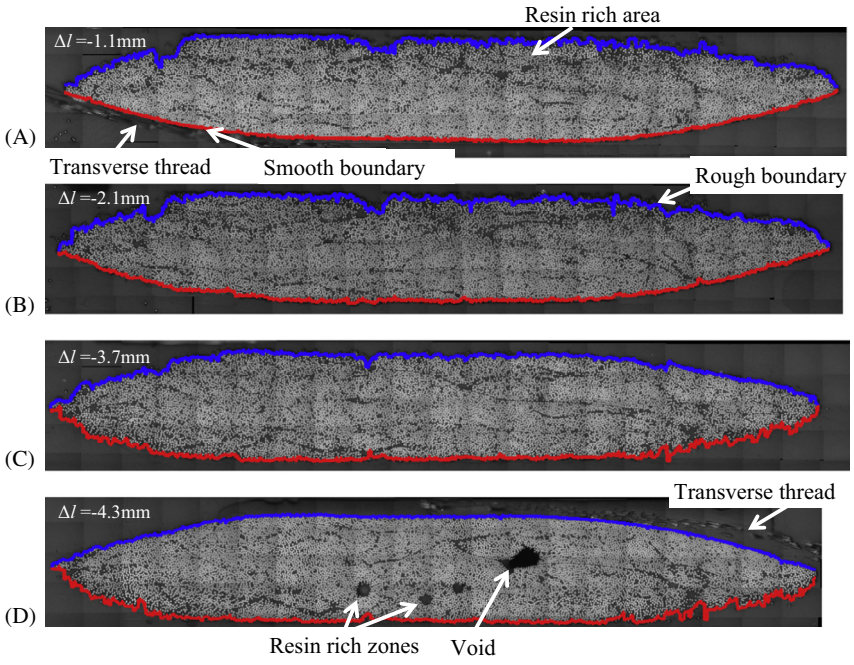

Fig. 6. Micrographs of a carbon fibre bundle cross-sectional area at different position, Δl, along the bundle path. (For interpretation of the references to colour in this figure legend, the reader is referred to the web version of this article.)

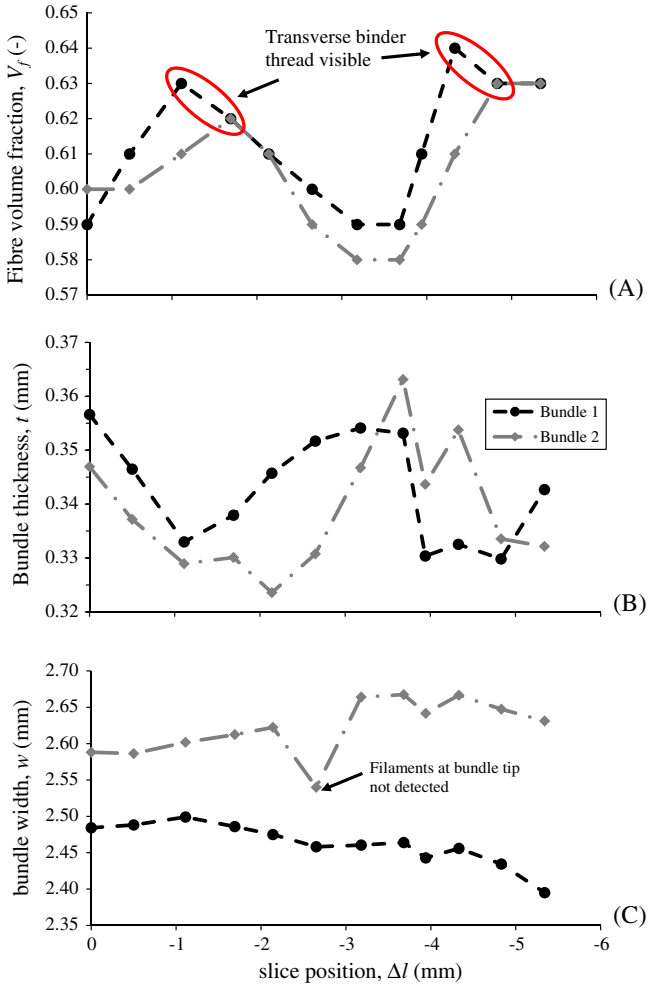

Fig. 7. (A) Average fibre volume fraction, (B) thickness and (C) width of two fibre bundles at different positions, Δl, along the bundle path. (For interpretation of the references to colour in this figure legend, the reader is referred to the web version of this article.)

estimated standard deviation in V_f for the samples analysed in this work seems to be independent of the slice position and ranges between 0.06 and 0.09.

The variation in fibre bundle dimension over approximately one unit cell length in this work was determined to be about 3.2% for the thickness and 1.3% for the bundle width. These variations are lower than presented for the randomly selected bundles found in twill weaves (14% and 6% for bundle thickness and width) [23] or non-crimp fabrics [34]. However, these changes in bundle dimensions will be affected by the fabric geometry and the amount of compaction [16]. It should be kept in mind that, depending on the bundle shape (e.g. lenticular), the bundle tips may not involve many filaments [35] and the width may therefore not significantly affect the average yarn V_f. For other properties such as permeability, the bundle tips may however significantly affect the resin flow.

4.2. Change in local fibre arrangements

The surface of the determined fibre bundle envelope is irregular in areas of lower local V_f, e.g. where no transverse binder thread is present (Fig. 6). It does, however, gradually change and becomes smooth in areas where the transverse thread is crossing. The interface between the fibre bundles and the thin glass threads is subjected to a higher normal force during mould closure which results in a local compaction of filaments. The filaments at the perimeter of the fibre bundle are able to move and rearrange along the path of the continuous glass thread. As the glass threads are coated with a thermoplastic material and have a low fibre count, movement of the filaments within these binder yarns are thought to be insignificant.

Analysing changes in local V_f on bundle cross-sections by means of Voronoi cell analysis, a higher V_f can be observed at the boundary where the transverse thread is present (Figs. 6D and 8D). This suggests that the filaments rearrange locally in response to the compaction force. It can also be seen, that this higher V_f is confined to a small area only and does not affect the filament arrangement in the entire fibre bundle. The affected zone has been estimated to have a width between 5 and 13 filament diameters for the analysed samples. This zone may be larger if samples with a higher global V_f, i.e. larger amount of compaction, are analysed.

The filament arrangements in the centre of the fibre bundle seem not to be affected by the local increase of V_f at the bundle perimeter. Areas of low or high V_f in the centre of the fibre bundle change gradually independent of the relative position of the weft thread. Within the fibre bundle, filament clusters of high V_f are present and separated by areas of low V_f. For this case, the filament arrangements were quantified in terms of distance and angle distributions between nearest neighbours and have been presented in an earlier study [16]. In the case of liquid resin flow during composite processing, it is likely that these areas of lower local V_f will act as main flow channels [36].

4.3. Effects of voids

In several bundle sections, voids were detected after abrading and re-polishing the sample surfaces (Fig. 6D). These voids are a result of air entrapment in the liquid resin matrix during the impregnation process. In maps of local V_f, these voids appear as areas of reduced V_f within the fibre bundle (Fig. 8D). As the voided area does not contain a matrix to fixate the filaments locally, filaments in this area may fracture during the polishing process. The voids therefore appear to contain no filaments when using optical microscopy, which may not be the case.

However, the trends in determined V_f in this work (Fig. 7A) seem not to be affected by the appearance of voids. It was observed that all detected voids originate in resin rich zones in between filaments (Fig. 9). The voids may change shape further along the fibre bundle path but they are surrounded by an area of increased V_f. These densely packed filaments are restricted in their movement [18]. This suggests that voids in the samples analysed here are formed only in areas of the fibre bundle which contain none or just a very limited amount of filaments.

The additional edge of the void may lead to poor image contrast at its circumference due to rounding effects of the filaments during polishing. The effect seems, however, to be small when analysing the changes in V_f over the width of a sample in adjacent bundle sections (Section 3.2). Therefore, no adjustments have been made to the analysis of the filament arrangements and these voids are treated as resin rich zones in the fibre bundle.

4.4. V_f effects on properties

The increase in V_f of the low crimp bundles at the crossing points with the binder threads will result in differences in local permeabilities [27]. Hence, the permeability in these zones will decrease which will increase the probability of gas entrapment during impregnating flow in these zones. On the other hand, the influence on the elastic mechanical properties in bundle direction is expected to be small. However, the observed increase in V_f at

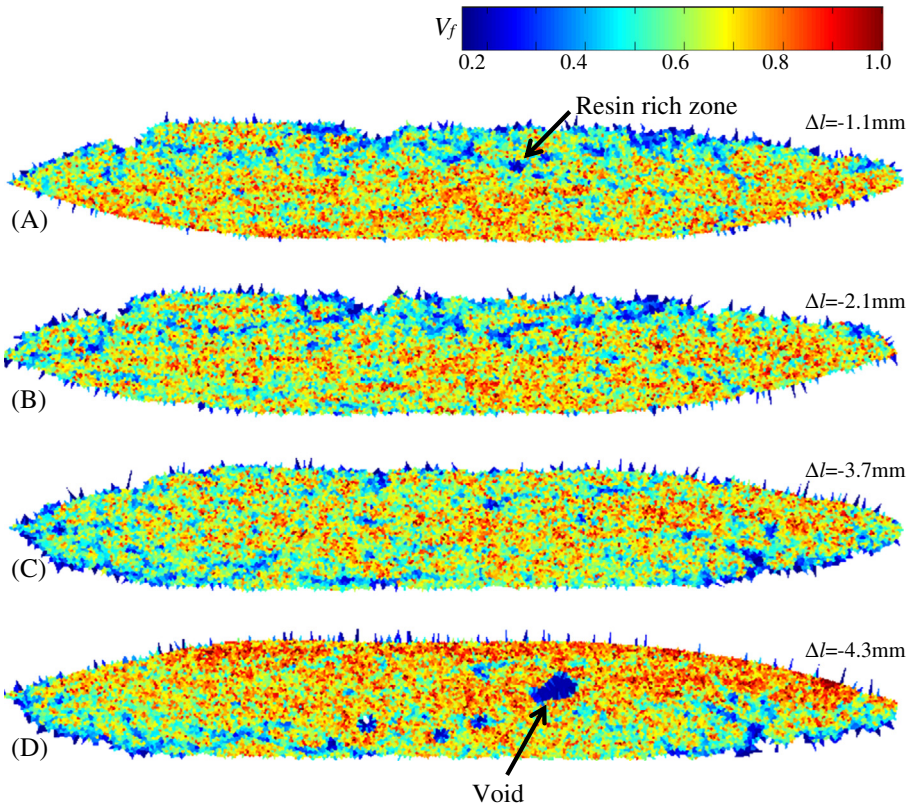

Fig. 8. Local fibre bundle volume fractions based on Voronoi cell tessellation at different position, Δl, along a fibre bundle path. (For interpretation of the references to colour in this figure legend, the reader is referred to the web version of this article.)

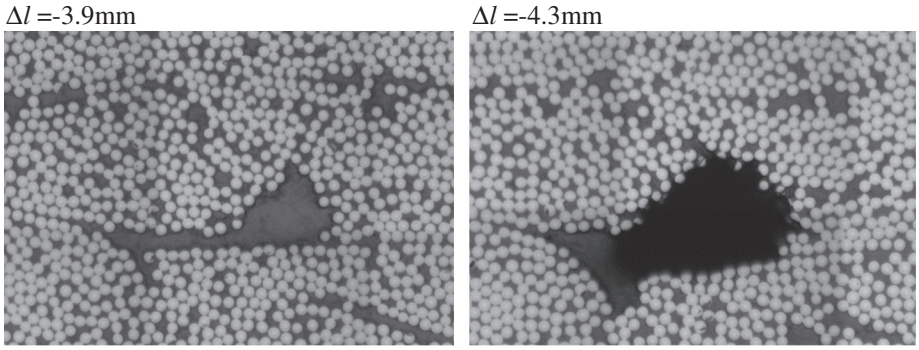

Fig. 9. Micrographs of a carbon fibre bundle cross-section before and after a void was detected.

the crossing of two fibre bundles is probably present in the case of a similar transverse weft bundle as well. Numerical simulations have shown that the stresses and strains in the bundles transverse to the loading direction are increased. Using the example of plain weave unit cells, damage initiation was always observed at the interface of transverse fibre bundles [37,38]. The increased V_f at the interface will lead to a more brittle material which may exceed the matrix strength between individual filaments locally [13]. Incorporating the observation of increased V_f at the fibre bundle interface rather than using random distributions in numerical meso-scale models [37] will probably further highlight this effect. It is therefore likely, that this causes cracks in [24,39] or around [40] the transverse fibre bundles to form during mechanical loading.

5. Concluding remarks

Changes in the random arrangement of filaments in fibre bundles were quantified along the bundle path. A local increase of the fibre volume fraction, V_f, towards the interface at cross-over points with transverse threads has been observed. In addition, local clusters of high V_f within a fibre bundle have been found which seem not to be affected by adjacent or interlaced fibre bundles. These clusters have different local filament arrangements and affect the fibre bundle properties differently. For example, the permeability in these high filament density clusters is decreased and may prevent full saturation with a liquid resin matrix during impregnation locally. If an area of low filament density is located within such a cluster of increased V_f, this may cause air entrapment

in this area. In addition, larger areas of low V_f may act as main fluid transport channels which dominate the fibre bundle permeability. This could lead to local race tracking inside the fibre bundle leading to gas entrapment within the adjacent clusters of higher V_f.

In addition, the increased V_f at the interface between two intersecting fibre bundles will lead to additional stress concentrations during mechanical loading as a result of an increased difference in stiffness. When numerically analysing the properties of a fibre bundle, the determined systematic and random changes in local V_f inside a fibre bundle can be taken into account for more accurate predictions.

The obtained results are specific for the analysed fabric at a single global V_f and should be confirmed on other fabric styles, different V_f and layered materials. It is thought, however, that the effect of local compaction of a fibre bundle at the interface between interlaced fibre bundles will also be found under different conditions. This effect is expected to be more pronounced when layers of transversely arranged bundles are compacted within a mould tool. On the other hand, the local compaction effects will be less distinct when bundles are aligned in parallel and nesting is allowed. But even in this case, at an increased amount of compaction, similar local effects at the bundle interface are probable to occur as the filaments within individual fibre bundles are limited to move individually due to long range entanglements. Unlike in the analysed case of a single bundle being compacted between two rigid plates, the compaction induced effects at the interface for layered materials will be shared between adjacent fibre bundles.

Acknowledgements

This work was supported by the Engineering and Physical Sciences Research Council [Grant Number: EP/IO33513/1], through the EPSRC Centre for Innovative Manufacturing in Composites (CIMComp) and by an EPSRC Doctoral Prize award hosted by the University of Nottingham.

References

[1] Mrse A, Piggott M. Compressive properties of unidirectional carbon fibre laminates: II. The effects of unintentional and intentional fibre misalignments. Compos Sci Technol 1993;46(3):219–27.
[2] Endruweit A, Long AC, Robitaille F, Rudd CD. Influence of stochastic fibre angle variations on the permeability of bi-directional textile fabrics. Compos Part A 2006;37(1):122–32.
[3] Tan H, Pillai KM. Fast liquid composite molding simulation of unsaturated flow in dual-scale fibre mats using the imbition characteristics of a fabric-based unit cell 10.
[4] Sriramula S, Chryssanthopoulos MK. Quantification of uncertainty modelling in stochastic analysis of FRP composites. Compos Part A 2009;40(11):1673–84.
[5] Long AC, Brown LP. Modelling the geometry of textile reinforcements for composites: TexGen. In: Boisse P, editor. Composite reinforcements for optimum performance. Cambridge: Woodhead Publishing Ltd.; 2011. p. 239–64.
[6] Zeng XS, Long AC, Gommer F, Endruweit A, Clifford M. Modelling compaction effect on permeability of 3D carbon reinforcements. In: 18th International conference on composite materials (ICCM18), Jeju Island, South Korea.
[7] El Said B, Green S, Hallett SR. Kinematic modelling of 3D woven fabric deformation for structural scale features. Compos Part A 2014;57:95–107.
[8] Park CH, Lebel A, Saouab A, Bréard J, Lee WI. Modeling and simulation of voids and saturation in liquid composite molding processes. Compos Part A 2011;42(6):658–68.
[9] Gebart BR. Permeability of unidirectional reinforcements for RTM. J Compos Mater 1992;26(8):1100–33.
[10] Guild FJ, Summerscales J. Microstructural image analysis applied to fibre composite materials: a review. Composites 1993;24(5):383–93.
[11] Gommer F, Wedgwood KCA, Brown LP. Stochastic reconstruction of filament paths in fibre bundles based on two-dimensional input data. Compos Part A 2015;76:262–71.
[12] Czabaj MW, Riccio ML, Whitacre WW. Numerical reconstruction of graphite/epoxy composite microstructure based on sub-micron resolution X-ray computed tomography. Compos Sci Technol 2014;105:174–82.
[13] Trias D, Costa J, Mayugo JA, Hurtado JE. Random models versus periodic models for fibre reinforced composites. Comput Mater Sci 2006;38(2):316–24.
[14] Requena G, Fiedler G, Seiser B, Degischer P, Di Michiel M, Buslaps T. 3D-Quantification of the distribution of continuous fibres in unidirectionally reinforced composites. Compos Part A 2009;40(2):152–63.
[15] Scott AE, Mavrogordato M, Wright P, Sinclair I, Spearing SM. In situ fibre fracture measurement in carbon–epoxy laminates using high resolution computed tomography. Compos Sci Technol 2011;71(12):1471–7.
[16] Gommer F, Endruweit A, Long AC. Analysis of filament arrangements and generation of statistically equivalent composite micro-structures. Compos Sci Technol 2014;99:45–51.
[17] Matveev MY, Long AC, Jones IA. Modelling of textile composites with fibre strength variability. Compos Sci Technol 2014;105:44–50.
[18] Mansfield EH, Purslow FRS, Purslow D. The influence of fibre waviness on the moduli of unidirectional fibre reinforced composites. RAE Technical Report; 1974.
[19] Eberhardt C, Clarke A. Fibre-orientation measurements in short-glass-fibre composites. Part I: automated, high-angular-resolution measurement by confocal microscopy. Compos Sci Technol 2001;61(10):1389–400.
[20] Davidson NC, Clarke AR, Archenhold G. Large-area, high-resolution image analysis of composite materials. J Microsc 1997;185(2):233–42.
[21] Luong B. FFT-based convolution. <www.mathworks.co.uk> [15.April 2013].
[22] Gommer F. Measurement data: Quantification of micro-scale variability in fibre bundles. <https://drive.google.com/folderview?id=0B-w_YqRvIONTQnUxbXhSd0NJa0k&usp=sharing> [02.April.2016].
[23] Olave M, Vanaerschot A, Lomov SV, Vandepitte D. Internal geometry variability of two woven composites and related variability of the stiffness. Polym Compos 2012;33(8):1335–50.
[24] Summerscales J, Russel PM. Observations on the fibre distribution and fibre strain in a woven fabric reinforcement. Adv Compos Lett 2004;13(3):135–40.
[25] Nakanishi Y, Matsumoto K, Kurashiki T, Zako M. Multiscale analysis of material damping properties for textile composites. In: 13th European Conference on Composite Materials (ECCM13), Stockholm.
[26] Okabe A, Boots B, Sugihara K. Spatial tessellations. Concepts and applications of voronoi diagrams. J. Wiley and Sons; 1992.
[27] Endruweit A, Gommer F, Long AC. Stochastic analysis of fibre volume fraction and permeability in fibre bundles with random filament arrangement. Compos Part A 2013;49:109–18.
[28] Silberschmidt VV. Effect of micro-randomness on macroscopic properties and fracture of laminates. J Mater Sci 2006;41(20):6768–76.
[29] Hellström JGI, Frishfelds V, Lundström TS. Mechanisms of flow-induced deformation of porous media. J Fluid Mech 2010;664:220–37.
[30] Pietsch T, Gindy N, Fahmi A. Nano- and micro-sized honeycomb patterns through hierarchical self-assembly of metal-loaded diblock copolymer vesicles. Soft Matter 2008;5:2188–97.
[31] Paluch B. Analysis of geometric imperfections affecting the fibers in unidirectional composites. J Compos Mater 1996;30(4):454–85.
[32] Zangenberg J, Larsen JB, Østergaard RC, Brøndsted P. Methodology for characterisation of glass fibre composite architecture. Plast Rubber Compos 2012;41(4–5):187–93.
[33] Bale H, Blacklock M, Begley MR, Marshall DB, Cox BN, Ritchie RO. Characterizing three-dimensional textile ceramic composites using synchrotron X-Ray micro-computed-tomography. J Am Ceram Soc 2011;95(1):392–402.
[34] Mattsson D, Joffe R, Varna J. Methodology for characterization of internal structure parameters governing performance in NCF composites. Compos B Eng 2007;38(1):44–57.
[35] Yurgartis SW, Morey K. Measurement of yarn shape and nesting in plain-weave composites. Compos Sci Technol 1993;46(1):39–50.
[36] Yazdchi K, Srivastava S, Luding S. Micro-macro relations for flow through random arrays of cylinders. Compos Part A 2012;43(11):2007–20.
[37] Matveev MY. Efects of variabilities on mechanical properties of textile composites PhD thesis. University of Nottingham; 2014.
[38] Zhou Y, Lu Z, Yang Z. Progressive damage analysis and strength prediction of 2D plain weave composites. Compos B Eng 2013;47:220–9.
[39] Ito M, Chou T-W. An analytical and experimental study of strength and failure behavior of plain weave composites. J Compos Mater 1998;32(1):2–30.
[40] Li L, Lomov SV, Yan X, Carvelli V. Cluster analysis of acoustic emission signals for 2D and 3D woven glass/epoxy composites. Compos Struct 2014;116:286–99.